The effect of an infinite plane-wave approximation on calculations for second-harmonic generation in a one-dimensional nonlinear crystal

A Letters Journal Exploring the Frontiers of Physics

May 2012

EPL, **98** (2012) 44004
doi: 10.1209/0295-5075/98/44004

www.epljournal.org

The effect of an infinite plane-wave approximation on calculations for second-harmonic generation in a one-dimensional nonlinear crystal

Jing Zhao and Li-Ming Zhao[(a)]

Center of Theoretical Physics, Department of Physics, Capital Normal University - Beijing 100048, China

received 14 March 2012; accepted in final form 19 April 2012
published online 22 May 2012

PACS 42.65.Ky – Frequency conversion; harmonic generation, including higher-order harmonic generation
PACS 42.70.Mp – Nonlinear optical crystals

Abstract – In this paper, the second-harmonic generation (SHG) in a one-dimensional nonlinear crystal that is embedded in air is investigated. Previously, the identical configuration was studied in Li Z. Y. *et al.*, *Phys. Rev. B*, **60** (1999) 10644, without the use of the slowly varying amplitude approximation (SVAA), but by adopting the infinite plane-wave approximation (PWA), despite the fact that this approximation is not quite applicable to such a system. We calculate the SHG conversion efficiency without a PWA, and compare the results with those from the quoted reference. The investigation reveals that conversion efficiencies of SHG as calculated by the two methods appear to exhibit significant differences, and that the SHG may be modulated by the field of a fundamental wave (FW). The ratio between SHG conversion efficiencies as produced by the two methods shows a periodic variation, and this oscillatory behavior is fully consistent with the variation in transmittance of the FW. Quasi-phase matching (QPM) is also studied, and we find that the location of the peak for SHG conversion efficiency deviates from $\Delta d = 0$, which differs from the conventional QPM results.

Introduction. – Means to obtain efficient frequency lasing is a topic of great interest in the field of nonlinear optics [1,2]. The traditional approach involves a birefringent crystal, which can satisfy the phase matching (PM) condition, to achieve high-efficiency second-harmonic generation (SHG). However, there are some restrictions in the choice of suitable materials, which arise from issues such as the walk-off effect. A more recent approach is based upon the quasi-phase matching (QPM) configuration [3–15], which utilizes the reciprocal lattice vector to compensate for wave vector mismatch between the fundamental wave (FW) and the second-harmonic wave (SHW); with this technique efficient SHG is easily obtained. In what follows, the periodic optical superlattice (POS), quasi-periodic optical superlattice (QOS), and aperiodic optical superlattice (AOS) are successively presented and shown to satisfy the QPM. Furthermore, the QOS and AOS can be designed to achieve multiple-wavelength SHG in a single sample. In addition, another optimized structure, dubbed non-periodic optical superlattice (NOS) [16] is proposed, and it is found to exhibit additional flexibility in its applications.

Optical waves propagating in nonlinear materials evolve according to the coupled-wave equations [3]. It is difficult to solve these equations rigorously, so that some approximations are often introduced to simplify the equations. Examples of such approximations include the slowly varying amplitude approximation (SVAA), infinite plane-wave approximation (PWA), and the non-depleted pump wave approximation (NPWA), among others. With the adoption of such approximations, the solutions to the coupled-wave equations are easy to obtain [3]. However, it is worth pointing out that these approximations are not always valid, and that they should only be adopted if appropriate on the basis of an actual scenario. For example, SVAA fails when the reflective SHW is not ignorable [17]. As regards the NPWA, the pump depletion cannot be neglected when the SHG conversion efficiency is relatively high [18]. Finally, the PWA neglects many factors restricted to pump wave, such as diffraction, etc. In ref. [19], the authors did not take into account reflections of the pump wave, and treated the pump wave simply

[(a)]E-mail: me_zlm@sohu.com

as a forward-propagating wave, which the authors justified by assuming that the pump was adjusted away from any resonances and the band edge. However, treatments that neglect pump wave reflections will fail in systems where the reflectance of the pump wave can be comparable with transmittance. In addition, some prior works have ventured beyond these sorts of approximations to calculate SHG and successfully attained accurate results [20–22]. Considering the case where a nonlinear crystal is embedded in air, the reflections of FW and SHW are so strong that they cannot be neglected, so that use of the PWA and SVAA are invalid for such a system. In ref. [17], the authors adopted a transfer matrix approach without incorporating the SVAA, but which instead used the PWA to study the SHG from a one-dimensional nonlinear crystal embedded in air. Therefore, it might be interesting to calculate the SHG in an approach which makes use of neither of these approximations (SVAA and PWA) for an identical configuration, and then compare the results obtained by the two methods.

With this inspiration, in this paper we apply a method to evaluate the SHG in the same structure as described in ref. [17], but without using the SVAA or PWA, and then compare the relevant results. We find that the SHG as studied using our method is quite different from that found in the previous publication: it is regulated by the field of the FW, and the ratio between its value and the value of the SHG as studied by the method in ref. [17], which presents a periodic vibration. We also find that this oscillation is fully consistent with the transmittance variations for the FW. In addition, the QPM for this case appears to be distinct from what is found in the conventional QPM situation.

Theory. – We examine a one-dimensional nonlinear crystal that is embedded in a homogeneous dielectric media. The incident light is normally launched upon the surface of sample from its left side. Under the non-depleted pump wave approximation, the FW (SHW) is governed by the following equations:

$$\frac{\mathrm{d}^2}{\mathrm{d}x^2}E_l^{(1)}(x)+k_l^{(1)2}E_l^{(1)}(x)=0, \tag{1}$$

$$\frac{\mathrm{d}^2}{\mathrm{d}x^2}E_l^{(2)}(x)+k_l^{(2)2}E_l^{(2)}(x)=-k_{20}^2\chi_l(x)E_l^{(1)2}(x), \tag{2}$$

where $k_{10}=\omega/c$, $k_{20}=2\omega/c$, $k_l^{(1)}=n_l^{1\omega}k_{10}$ and $k_l^{(2)}=n_l^{2\omega}k_{20}$, c is the speed of light in a vacuum, and $k_l^{(1)},k_l^{(2)}$ $(n_l^{1\omega},n_l^{2\omega})$ represent the wave vectors (refractive indices) for the FW (SHW) in the l-th layer of the material, respectively.

The electric field of the FW in the l-th layer can be expressed in the form

$$\begin{aligned}E_l^{(1)}(x) \;=\; & A_l^{(1)}\exp[ik_l^{(1)}(x-x_{l-1})]\\ & +B_l^{(1)}\exp[-ik_l^{(1)}(x-x_{l-1})].\end{aligned} \tag{3}$$

Here $x_1=0$, $x_l=x_{l-1}+d_l(l=2,3,\ldots)$ and d_l is the thickness of the l-th layer. $A_l^{(1)}$ and $B_l^{(1)}$ represent the amplitudes for the forward and backward propagating FW in the l-th layer. By using the continuous condition of the electric and magnetic fields at the interface, we derive

$$\begin{pmatrix}A_{l+1}^{(1)}\\ B_{l+1}^{(1)}\end{pmatrix}=\begin{pmatrix}t_{11}^{(l)} & t_{12}^{(l)}\\ t_{12}^{(l)*} & t_{11}^{(l)*}\end{pmatrix}\begin{pmatrix}A_l^{(1)}\\ B_l^{(1)}\end{pmatrix}=\hat{T}_l\begin{pmatrix}A_l^{(1)}\\ B_l^{(1)}\end{pmatrix}$$

with the elements

$$t_{11}^{(l)}=\frac{k_{l+1}^{(1)}+k_l^{(1)}}{2k_{l+1}^{(1)}}e^{ik_l^{(1)}d_l},\qquad t_{12}^{(l)}=\frac{k_{l+1}^{(1)}-k_l^{(1)}}{2k_{l+1}^{(1)}}e^{-ik_l^{(1)}d_l}.$$

$\hat{T}_l=\begin{pmatrix}t_{11}^{(l)} & t_{12}^{(l)}\\ t_{12}^{(l)*} & t_{11}^{(l)*}\end{pmatrix}$ is the transfer matrix of the l-th layer. Assuming that the total number of layers of the configuration is N, the overall transfer matrix can be obtained from cascading result of the successive individual $\hat{T}_l$. Considering the boundary condition $B_N^{(1)}=0$ and the amplitude of pump wave $A_1^{(1)}$, the amplitudes $A_l^{(1)}$ and $B_l^{(1)}$ of every layer can be determined.

The electric field for the SHW in the l-th layer can be described by

$$\begin{aligned}E_l^{(2)}(x) \;=\; & A_l^{(2)}\exp[ik_{lx}^{(2)}(x-x_{l-1})]\\ & +B_l^{(2)}\exp[-ik_{lx}^{(2)}(x-x_{l-1})]\\ & +C_l^{+}\exp[i2k_l^{(1)}(x-x_{l-1})\\ & +C_l^{-}\exp[-i2k_l^{(1)}(x-x_{l-1})]\\ & -\frac{2k_{20}^2\chi_l}{(k_l^{(2)})^2}A_l^{(1)}B_l^{(1)},\end{aligned} \tag{4}$$

where $A_l^{(2)}$ and $B_l^{(2)}$ represent the amplitudes for the forward and backward SHW in the l-th layer. Upon substitution of eqs. (3) and (4) into eq. (2), we get

$$C_l^{+}=\frac{-k_{20}^2\chi_l A_l^{(1)2}}{k_l^{(2)2}-4k_l^{(1)2}}, \tag{5}$$

$$C_l^{-}=\frac{-k_{20}^2\chi_l B_l^{(1)2}}{k_l^{(2)2}-4k_l^{(1)2}}. \tag{6}$$

Considering the continuous condition of the electric and magnetic fields at the interface, $A_l^{(2)}$ and $B_l^{(2)}$ can be evaluated via the matrix

$$\begin{pmatrix}A_{l+1}^{(2)}\\ \mathrm{B}_{l+1}^{(2)}\end{pmatrix}=\begin{pmatrix}q_{11}^{(l)} & q_{12}^{(l)}\\ q_{12}^{(l)*} & q_{11}^{(l)*}\end{pmatrix}\begin{pmatrix}A_l^{(2)}\\ B_l^{(2)}\end{pmatrix}+\begin{pmatrix}f_{l+}\\ f_{l-}\end{pmatrix}$$

and

$$q_{11}^{(l)} = \frac{k_{l+1}^{(2)} + k_l^{(2)}}{2k_{l+1}^{(2)}} e^{ik_l^{(2)} d_l}, \quad q_{12}^{(l)} = \frac{k_{l+1}^{(2)} - k_l^{(2)}}{2k_{l+1}^{(2)}} e^{-ik_l^{(2)} d_l},$$

$$\begin{aligned} f_{l\pm} = & -\frac{k_l^{(2)} \pm 2k_l^{(1)}}{2k_l^{(2)}} C_l^+ - \frac{k_l^{(2)} \mp 2k_l^{(1)}}{2k_l^{(2)}} C_l^- \\ & + \frac{k_l^{(2)} \pm 2k_{l-1}^{(1)}}{2k_l^{(2)}} C_{l-1}^+ e^{i2k_{l-1}^{(1)} d_{l-1}} \\ & + \frac{k_l^{(2)} \mp 2k_{l-1}^{(1)}}{2k_l^{(2)}} C_{l-1}^- e^{-i2k_{l-1}^{(1)} d_{l-1}} + \frac{k_{20}^2 \chi l}{k_l^{(2)}} A_l^{(1)} B_l^{(1)} \\ & - \frac{k_{20}^2 \chi_{l-1}}{k_{l-1}^{(2)}} A_{l-1}^{(1)} B_{l-1}^{(1)}. \end{aligned}$$

Accounting for the initial condition $A_1^{(2)} = 0$ and $B_N^{(2)} = 0$, the conversion efficiencies of the forward and backward SHG will then be given by

$$\eta_{forth} = \frac{n_N^{(2)} \left| A_N^{(2)}(x_{N-1}) \right|^2}{n_1^{(1)} \left| A_1^{(1)} \right|^2}, \tag{7}$$

$$\eta_{back} = \frac{n_1^{(2)} \left| B_1^{(2)}(x_1) \right|^2}{n_1^{(1)} \left| A_1^{(1)} \right|^2}. \tag{8}$$

Analysis. – In our investigation, the sample modeled is a homogeneous crystal made of $LiNbO_3$, with a crystal length of $d = 200\,\mu$m, which is embedded in air. The wavelength of incident light is $\lambda = 1.064\,\mu$m, and its intensity is set to $I = 1.328 \times 10^9\,\mathrm{W/m^2}$, which corresponds to $|E_1^{(1)}(x_1)|^2 = 1.00\,\mathrm{V^2}/\mu\mathrm{m}^2$. The nonlinear coefficient d_{33} is $47.0\,p$m/V, and the refractive indices for the FW and SHW in the crystal are taken from ref. [23]. Figure 1 shows the SHG conversion efficiencies as calculated by our method (solid line) and as calculated in ref. [17] (dashed line) vary with phase mismatch ($\Delta k = 2k_1 - k_2$). In the figure, comparisons are shown for the (a) total, (b) backward, and (c) for the forward SHG conversion efficiency. It is clearly evident in fig. 1(a)–(c) that the locations for all SHG peak values in each of the two methods deviate from $\Delta k = 0$. This is in contrast to the results from conventional PM. In the results, there are two peaks, situated at the same locations: $\Delta k = -0.007$ and $\Delta k = 0.006$, for total and forward SHG. However, the peak locations differ for the backward SHG, as seen in fig. 1(b). For the dashed curve, the peak values remain at $\Delta k = -0.007$ and $\Delta k = 0.006$, while the locations for the solid curve are shifted to $\Delta k = 0.005$ and $\Delta k = -0.005$. This implies that the difference in peak locations from the conventional PM is mainly due to the avoidance of the SVAA, where the reflected SHW is not considered, and that the interference

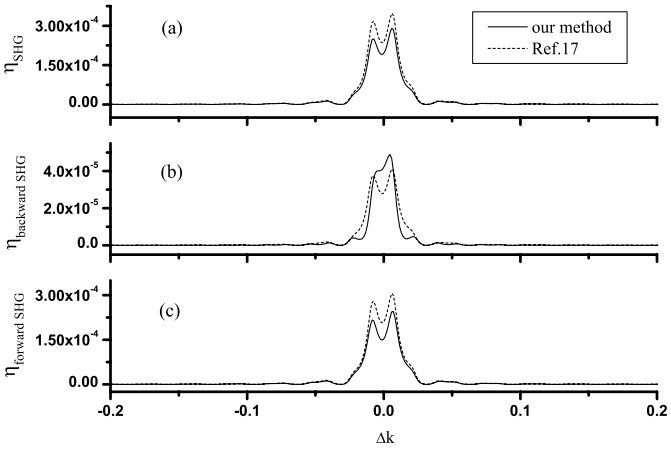

Fig. 1: Variation of the SHG conversion efficiencies with Δk, as calculated by our method (solid line) and in ref. [17] (dashed line): (a) total, (b) backward and (c) forward SHG conversion efficiency.

effect between the transmitted and reflected SHW leads to the peak deviating from $\Delta k = 0$. For other choices of crystal length values, the peak locations for forward and total SHG remain consistent for both approaches, but the backward SHG peak location still shows a difference. Moreover, it is worth noting that the locations for the SHG peak values do change as a function of the crystal length.

A one-dimensional POS is studied, in which the structure is composed of repeated inverted poled layers of $LiNbO_3$, and the structure is embedded in air. We assume that the number of layers is chosen as $N = 52$, the thickness of each crystal layer is d_l, and $\Delta d = d_l - l_C$ denotes the deviation from the coherent length l_C, while all other necessary parameters of this system are the same as those as used in producing fig. 1. The dependence of SHG conversion efficiency on Δd is shown in fig. 2(a) and (b), respectively for the SHG conversion efficiency calculated in the method of ref. [17] (solid curve in (a)) and ours (solid curve in (b)), the smooth curve represents the SHG conversion efficiency evaluated in the conventional sample that is embedded in a nonlinear non-polarized $LiNbO_3$ medium. In order to elaborately present the variation of SHG conversion efficiency, two illustrations showing in part the changes of the SHG conversion efficiency and transmittance are introduced, the upper layers give the dependence of the SHG conversion efficiencies on Δd, and the lower layers show the transmittance. It is clearly seen that the smooth curve has only one peak situated at $\Delta d = 0$, yet the case of QPM is quite different from that for the solid curves. It is clearly seen from fig. 2(a) that the solid curve oscillates periodically around the conventional one, and curve-outline is the same with the smooth one. Considering the interference of the forward and backward SHW, the transmittance of SHW is presented in the lower layer of the illustration, and obviously, the variation behavior of SHG conversion efficiency is fully consistent

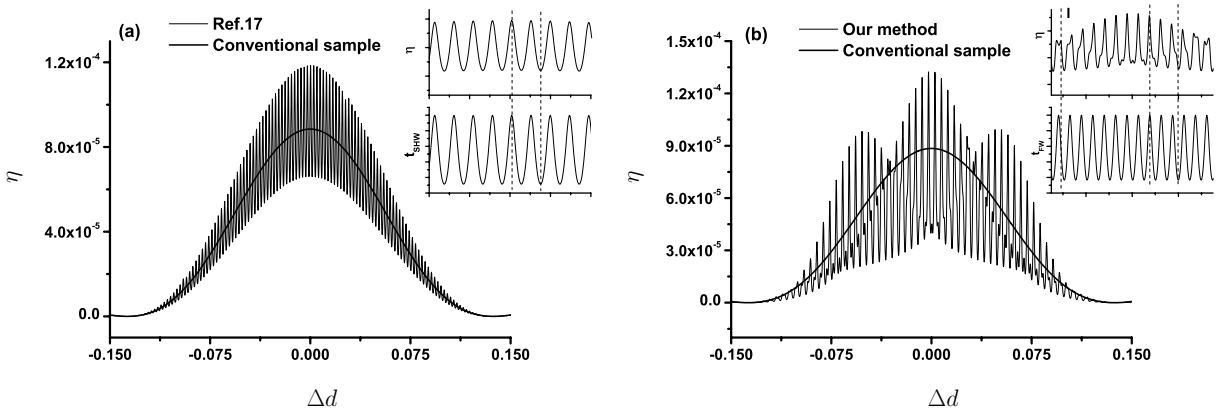

Fig. 2: Variation of the SHG conversion efficiencies with Δd ($\Delta d = d_l - l_C$), (a) for the conversion efficiency calculated in the method of ref. [17] (solid curve), the illustration shows in part the variation of it (upper layer) and the transmittance of SHW (lower layer) with Δd; (b) for SHG conversion efficiency calculated in our method (solid curve), the illustration displays the dependence of it (upper layer) and transmittance of FW (lower layer) on Δd; the smooth curve denotes SHG conversion efficiency for conventional sample.

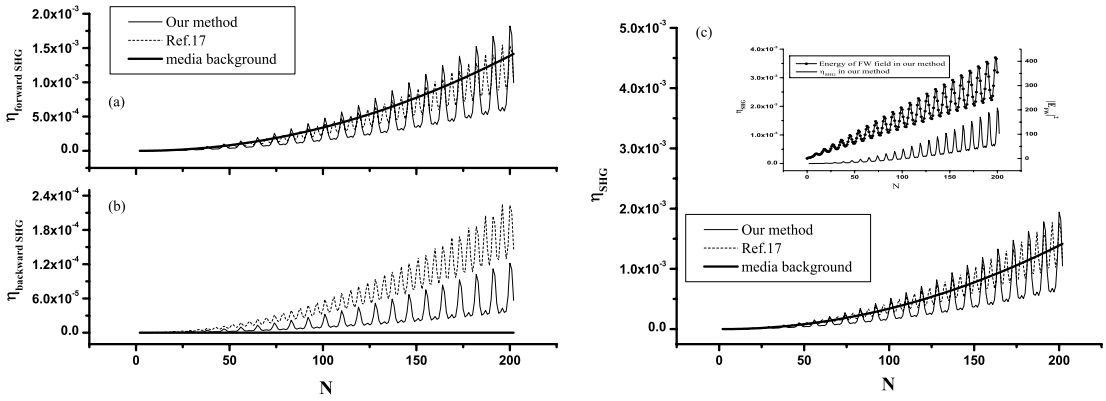

Fig. 3: SHG conversion efficiencies *vs.* N, calculated for conventional sample (smooth line) and for a sample embedded in air (the two oscillatory lines, our method (solid line) and method from ref. [17] (dashed line)): (a) forward, (b) backward, and (c) total SHG. The inserted picture in (c) shows the conversion efficiency (solid curve) and energy of the FW field (the circled curve) as found in our method.

with the transmittance, and the SHG conversion efficiency reaches the peak value when the transmittance resonance occurs. While for fig. 2(b), the solid curve also vibrates periodically around the traditional scenario, but the curve-outline is different from the conventional one, there exists two clusters of peaks which deviate from the conventional curve. To investigate the chief causes of the two clusters of peaks, the transmittance of FW is presented in the lower layer of the illustration. It is clearly seen that the curve-outline for SHG conversion efficiency is almost consistent with the transmittance, but there are some peaks such as the peak named I deviating from the resonant peaks of the FW. And we find that these peaks actually correspond to the resonant peaks of SHW. At this time, the origin of the two clusters of peaks is clear for us, in fact, they correspond to the transmittance resonance for the FW and SHW, this point is verified by the simulation. Using other values of N, similar results can be obtained, except for the specific locations for the peak of SHG.

We have calculated the SHG conversion efficiency as a function of the number of layers N, where N is taken from 2 to 202 and $d_l = l_C$, with the results shown in fig. 3. In that figure, the smooth curve denotes the SHG conversion efficiency in conventional sample, and the two oscillatory curves represent the SHG conversion efficiencies in a sample embedded in air, as calculated by using our method (solid curve) as well as that of ref. [17] (dashed curve). Obvious differences are seen in the variations of the three curves in fig. 3(a)–(c). In fig. 3(b), the backward SHG in the conventional sample is zero, as opposed to the result from the case where the crystal is embedded in air (solid and dashed curves), and the value calculated by the method in ref. [17] (dashed curve) is always higher than the result from our method (solid curve). For the forward

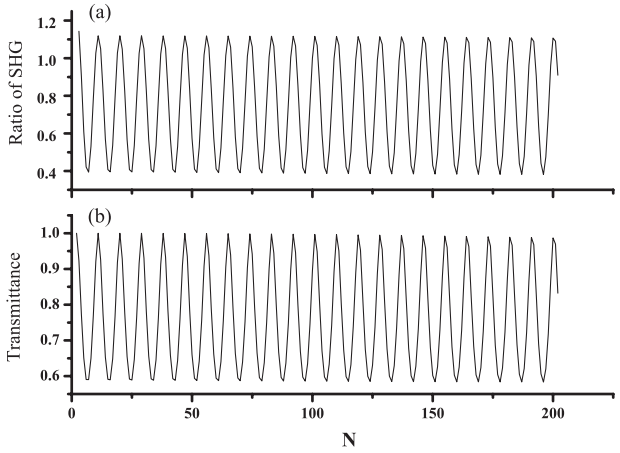

Fig. 4: (a) Ratio of SHG conversion efficiency and (b) transmittance as functions of N.

and total SHG in fig. 3(a) and (c), the SHG conversion efficiencies increase with the growth of the crystal layers number; this indicates that the increasing SHG arises from satisfying the QPM condition. In addition, the solid and dashed curves oscillate around the smooth curve with different values and periods, where the oscillatory period for the solid line (9.000) is twice that of the dashed line (4.500). The oscillations in the dashed curve mainly originate from the interference of forward and backward SHWs. While the variations in the solid curve are mainly attributed to the modulation of the FW field, which is verified in the inserted picture in fig. 3(c), where the picture shows that the variation of the total conversion efficiency (solid curve) in our method is fully consistent with the energy of the FW field (circled curve), *i.e.* that the SHG reaches its peaks and troughs when the energy of the FW field reaches its peaks and troughs, and the SHG reaches peak values when transmittance resonance occurs. With increasing N, the amplitude of oscillation grows, and the difference in conversion efficiency as calculated by the two different methods corresponds to this growth, with a maximum difference at $N = 197$ where $\Delta\eta = |\eta_{\text{ref.}[17]} - \eta_{our\,way}| = 2.89 \times 10^{-4}$.

To evaluate the effect of the modulation of the FW field on the SHG, we can define a $ratio = \eta_{our\,way}/\eta_{\text{ref.}[17]}$. In order to compare the SHG that is calculated in the two methods, that ratio is plotted in fig. 4(a), while fig. 4(b) shows a plot of the transmittance of the FW as it varies with N. Clearly evident in the figure, the SHG ratio ranges from 0.381 to 1.143 and performs a periodic oscillation, while the transmittance also oscillates periodically from 0.583 to 1.000, and the two oscillatory behaviors are fully correlated. That is to say, the SHG ratio reaches a peak (or trough) when the transmittance is at a peak (or trough), and when transmittance resonance occurs the SHG ratio attains its maximum value.

Summary. – In conclusion, we have investigated SHG in a one-dimensional nonlinear crystal that is embedded in air by adopting a method that does not make use of the PWA or the SVAA, and have compared the results with corresponding results that are derived from the method proposed by ref. [17], which investigates the same configuration without resorting to the SVAA, but which uses the PWA that is not applicable to the system. Our results indicate that the SHG as calculated by our method presents significant differences: it is modulated by the field of the FW, and the ratio between its value and the SHG as calculated by the method in ref. [17] exhibits a periodic oscillation, which is consistent with the oscillation of the FW transmittance. In addition, the QPM is found to differ from that in the conventional QPM scenario.

* * *

This work was supported by the National Natural Science Foundation of China (NNSFC) under grant 10874124 and 11004139, the Natural Science Foundation of Beijing under grant 1102012 and PHR (IHLB) from Beijing.

REFERENCES

[1] Franken P. A., Hill A. E., Peters C. W. and Weinreich G., *Phys. Rev. Lett.*, **7** (1961) 118.
[2] Armstrong J. A., Bloembergen N., Ducuing J. and Pershan P. S., *Phys. Rev.*, **127** (1962) 1918.
[3] Shen Y. R., *The Principles of Nonlinear Optics* (Wiley, New York) 1984.
[4] Stivala S., Busacca A. C., Curcio L., Oliveri R. L., Riva-Sanseverino S. and Assanto G., *Appl. Phys. Lett.*, **96** (2010) 111110.
[5] Zhang Y., Qi Z., Wang W. and Zhu S. N., *Appl. Phys. Lett.*, **89** (2006) 171113.
[6] Rose A. and Smith D. R., *Phys. Rev. A*, **84** (2011) 013823.
[7] Pasquazi A. and Assanto G., *Phys. Rev. A*, **80** (2009) 021801.
[8] Busacca A. C., Sones C. L., Eason R. W. and Mailis S., *Appl. Phys. Lett.*, **84** (2004) 4430.
[9] Song J. H., Freeman A. J., Bera T. K., Chung I. and Kanatzidis M. G., *Phys. Rev. B*, **79** (2009) 245203.
[10] Zhao L.M. and Gu B. Y., *Appl. Phys. Lett.*, **88** (2006) 122904.
[11] Xu P., Zhu S. N., Yu X. Q., Ji S. H., Gao Z. D., Zhao G., Zhu Y. Y. and Ming N. B., *Phys. Rev. B*, **72** (2005) 064307.
[12] Li J. J., Li Z. Y. and Zhang D. Z., *Phys. Rev. B*, **77** (2008) 195127.
[13] Rakher M. T., Ma L., Davanço M., Slattery O., Tang X. and Srinivasan K., *Phys. Rev. Lett.*, **107** (2011) 083602.
[14] Fischer R., Neshev D. N., Saltiel S. M., Sukhorukov A. A., Krolikowski W. and Kivshar Y. S., *Appl. Phys. Lett.*, **91** (2007) 031104.
[15] Zhao L. M., Gu B. Y., Zhou Y. S. and Wang F. H., *J. Phys: Condens. Matter*, **15** (2003) 4889.
[16] Chen X., Wu F., Zeng X., Chen Y., Xia Y. and Chen Y., *Phys. Rev. A*, **69** (2004) 013818.

[17] Li Z. Y., Gu B. Y. and Yang G. Z., *Phys. Rev. B*, **60** (1999) 10644.
[18] Kong X., Chen X. and Xia Y., *Appl. Phys. B*, **91** (2008) 479.
[19] Martorell J. and Corbalan R., *Opt. Commun.*, **108** (1994) 319.
[20] Rustagi K. C., Mehendale S. C. and Meenakshi S., *IEEE J. Quantum Electron.*, **18** (1982) 1029.
[21] Fejer M. M., Magel G. A., Jundt D. H. and Byer R. L., *IEEE J. Quantum Electron.*, **28** (1992) 2631.
[22] Li J. J., Li Z. Y. and Zhang D., *Phys. Rev. E*, **75** (2007) 056606.
[23] Dmitriev V. G., Gurazdyan G. G. and Nikogosyan D. N., *Handbook of Nonlinear Optical Crystals* (Springer, Berlin) 1997.